RSC Advances

PAPER

Effect of mechanical compression on Cu(In,Ga)Se_2 films: micro-structural and photoluminescence analysis

Cite this: *RSC Adv.*, 2014, **4**, 5141

Zhengfei Wei,*[a] S. Senthilarasu,[ac] Michael V. Yakushev,*[b] Robert W. Martin[b] and Hari M. Upadhyaya*[a]

Received 5th September 2013
Accepted 9th December 2013

DOI: 10.1039/c3ra44908d

www.rsc.org/advances

Cu(In,Ga)Se_2 (CIGS) thin films were deposited by a two-step process on Mo-coated soda-lime glass substrates. The CuInGa (CIG) precursors were prepared in an in-line evaporation system at room temperature, and then selenised at 500 °C. The two-step processed CIGS films were mechanically compressed at 25 MPa to improve their optoelectronic properties, which were verified by photoluminescence (PL). The surface and structural properties were compared before and after compression. The mechanical compression has brought changes in the surface morphology and porosity without changing the structural properties of the material. The PL technique has been used to reveal changes in the electronic properties of the films. PL spectra at different excitation laser powers and temperatures were measured for as-grown as well as compressed samples. The PL spectra of the as-grown films revealed three broad and intense bands shifting at a significant rate towards higher energies (*j*-shift) with the increase in excitation power suggesting that the material is highly doped and compensated. At increasing temperature, the bands shift towards lower energies, which is a characteristic of the band tails generated by spatial potential fluctuation. The compression increases the intensity of energy bands by an order of magnitude and reduces the *j*-shift, demonstrating an improvement of the electronic properties.

Introduction

The renewable energy generation market expansion through thin film photovoltaic technologies can be achieved by optimisation of the large scale manufacturing processes and by improving the module efficiency significantly. The Cu(In,Ga)Se_2 (CIGS) solar cells have already demonstrated high energy conversion efficiencies,[1–3] long term durability and cost effective production methods which make them competitive to current silicon-based PV technologies. CIGS solar cells are generally made by different vacuum[1–6] and non-vacuum techniques.[4,7] The vacuum techniques are superior to the non-vacuum due to a better control they have over the film growth leading to less defect formation, which results in a high performance of the device. The vacuum techniques such as 'three-stage' co-evaporation process[1,2] are generally used for most efficient CIGS solar cells as of today.[3] Alternatively, two-step process[5–17] is also gaining importance and has been applied to get reasonably efficient CIGS solar cells. Companies such as Frontier Solar, TSMC now have their expansion plans on mass production.[16,17] The controllability of various parameters in the three-stage growth process can bring complexities for CIGS solar cell manufactures *viz.* high processing temperature (500–600 °C), high vacuum (10^{-6}–10^{-5} mbar). Whilst, two-step process is less complicated and has shown a considerable improvement in the quality of thin films and the efficiency of the devices recently.[10]

Selenisation of metallic precursors using Se/N_2 (ref. 4, 5, 7 and 14) or H_2Se (ref. 9, 10 and 15) environment is considered as a simple and promising two-step approach to produce good quality absorber and high efficiency CIGS solar cells. The low-temperature, low-vacuum and mechanical compression methods have attracted attention in the two-step process of CIGS preparation due to their manufacturing advantage and the improved quality of thin film preparation.[5–8,11] However, in the scaling-up process, CIGS thin films often suffer from the inhomogeneity problems over large area. These are the main deviations observed from the composition uniformity, which is attributed to the unwanted defects and defect clusters.[18] Such defects play an important role in reducing the conversion efficiency, as they become potential trap sites for the carriers. Moreover, the intermixing and alloy formation in the Cu–In

[a]*Energy Conversion Laboratory (ECL), Institute of Mechanical Process and Energy Engineering (IMPEE), School of Engineering and Physical Sciences, Heriot-Watt University, Riccarton, Edinburgh, EH14 4AS, UK. E-mail: zw60@hw.ac.uk; h.m.upadhyaya@hw.ac.uk; Fax: +44 (0)1314513126; Tel: +44 (0)1314514381*

[b]*Department of Physics, SUPA, Strathclyde University, 107 Rottenrow, Glasgow, G4 0NG, UK. E-mail: michael.yakushev@strath.ac.uk*

[c]*Environment and Sustainability Institute (ESI), University of Exeter, Penryn, Cornwall TR10 9EZ, UK*

precursor layers also cause the non-uniformity of the layers during the low temperature (130 °C) and low pressure (10 mbar) deposition methods.[5,7] Several methods such as hydrogen (H_2) annealing, chemical treatment and mechanical compression have been attempted to address these problems and to suppress the defects for a good quality CIGS absorber formation.[11,19–22]

Mechanical compression is generally used in the material processing engineering to achieve high uniformity and high compactness of thin films, especially in low temperature processed dye-sensitised solar cell. This technique improves the necking between the porous TiO_2 particles and an improvement in the adhesion of the materials on the flexible substrates for dye sensitised solar cells applications.[23,24]

In our recent publication,[14] solar cells based on CIGS films deposited using two-step process without compression showed a low solar cell efficiency of ~3% due to high level of defects and porosity present in the material. A better device performance can be achieved using the CIGS films grown with less voids and cracking, larger grains and higher uniformity. The mechanical compression technique was previously used on CIGS films which showed reduction in the films porosity and improvement in the layer uniformity.[11] Although the changes on surface morphology and crystallinity due to compression have been investigated in previous studies, the electronic properties and defect nature of the compressed CIGS absorber layers were not fully addressed.

In this article, PL analysis was used to collect important information on the defect nature and mechanisms of radiative recombination.[25] Furthermore, the influence of the mechanical compression on the structural and optoelectronic properties of two-step processed CIGS films has revealed some interesting facts which have been investigated and correlated with the PL data.

Experimental techniques

Stacked CuInGa (CIG) metal precursor layers were grown using an in-line co-evaporation system[14] using three pairs of sources *viz.* copper (LTS Chemicals, 99.99%), indium (LTS Chemicals, 99.999%) and gallium (LTS Chemicals, 99.999%). These point molecular beam epitaxy (MBE) sources on 1 μm thick Mo ($\leq$0.20 Ω sq^{-1}) coated soda-lime glass were used to deposit layers of CIG precursor films, which ensured a good uniformity of the layers. The newly designed and built in-line co-evaporation system consists of two deposition zones which are separated by a metal shield between Cu and Ga–In sources for necessary deposition control in selective regions and avoiding cross contamination. The CIG precursor layer was then selenised in a two-temperature-zone quartz tube reactor furnace. Selenium vapours were generated from Se pellets (Sigma Aldrich 99.999%) at 300 °C in the first temperature zone. The Nitrogen (N_2) was used as a carrier gas to transport selenium vapours to the second deposition zone. The CIG precursor was selenised at about 500 °C to form $Cu(In,Ga)Se_2$ layers. Then, the CIGS films were cut into 1 cm^2 samples and compressed using a mechanical compression machine to apply 2.5 tons force which equals 25 MPa pressure onto the sample.

As deposited and mechanically compressed CIGS layers were analysed using different characterisation techniques described as follows to understand the structure, their surface morphology and defects nature. The surface morphology of CIGS was studied with the help of an FEI Quanta 3D Dual Beam (Ion and Electron) field emission gun scanning electron microscope (FEG-SEM). The crystalline structure was measured using a Bruker AXS D8 Advance glancing X-ray diffractometer (XRD). Temperature and excitation power resolved photoluminescence (PL) measurements before and after compression were carried out on the CIGS thin films to understand the mechanisms of radiative recombination, nature of the defects, and effects of compression on the defect properties. The PL measurements were performed using a closed-cycle cryostat, at temperatures from 5 to 300 K. An Ar^+ laser (514 nm) was used for excitation. PL emission was focused on the entrance slits of a 1 m spectrometer and detected by an InGaAs photomultiplier tube (PMT sensitive within the range from 950 to 1650 nm). Laser excitation power was varied from 0.2 to 20 mW which corresponds to power densities ramping from 0.16 to 16 W cm^{-2}.

Results and discussion

Fig. 1 shows the surface morphology of CIGS films before and after compression. The SEM picture (Fig. 1a) reveals the porous and less compact nature of the as-grown film. It is believed that the non-uniformity of the mixing Cu, In and Ga atoms leads to different reaction rates across the sample in the presence of selenium. This leads to regions of non-homogeneous growth of the films. This unevenness in the growth pattern can lead to significant stresses in the film, and the grain boundaries created between bigger and smaller grains. The disordered nature of this porous growth can be seen in the cross sectional SEM image (Fig. 1c). After the mechanical compression, the surface (Fig. 1b) becomes smoother and more condensed as expected. The randomly oriented granular structures were

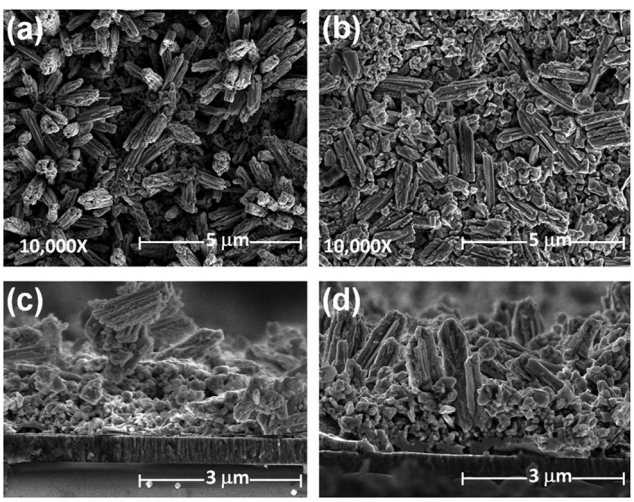

Fig. 1 SEM micrographs of CIGS film surface and cross-section: (a and c) as grown film and (b and d) after compression.

brought closer by compression of the as-grown films without changing its grain size. Their structure becomes columnar and the surface morphology of the films becomes an arrangement of bundles of slender and small grains arranged in a pillar shape (Fig. 1d). Oriented grains after compression have become more apparent suggesting a change in the morphology of the samples. At the bottom of the compressed film, a thin jointed layer appears which is indicative of providing additional compactness and can reduce the shunt resistance of the device. The compression on the loosely connected bundles of grains brings them together and reduces the porous nature of the as-grown films without changing its orientation.

X-ray diffraction was performed on the CIGS film samples to detect any significant changes or appearance of new phases of CIGS under the effect of compression. The XRD spectra CIGS (JCPDS 35-1102) grown on Mo coated glass substrates shows the preferential orientations of (112) and (220/204) phases confirming the formation of crystalline CIGS. Fig. 2 shows the comparison of XRD spectra of CIGS films before and after compression. The XRD spectra of the CIGS films before and after compression reveal similar widths of the peaks (full width at half maximum, FWHM). This suggests that the structural quality of the films has not been affected by the compression. The ratios of intensities of the peaks are also not affected by the compression demonstrating that compression does not change the main orientation of the grains. It was also evident from XRD studies that CIGS phases were unchanged after the compression.

Fig. 3a shows PL spectra of the as-grown and compressed films. It can be seen that the compression significantly increases the intensity of PL emission. In order to compare these spectra at the same scale, the spectrum from the as-grown films was factored appropriately as shown in Fig. 3b. This figure also shows a PL spectrum measured in $Cu(In,Ga)Se_2$ thin films with similar gallium content [Ga]/[Ga] + [In] = 0.3, and used here as a reference. The reference films deposited on Mo coated soda-lime glass substrates to produce solar cells with

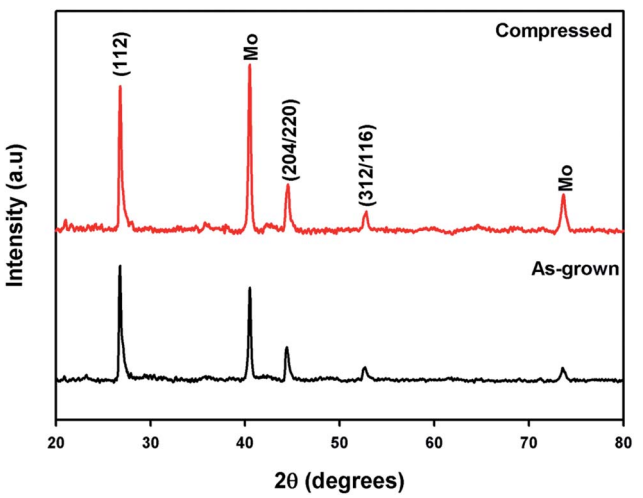

Fig. 2 The XRD patterns of the CIGS films before and after compression.

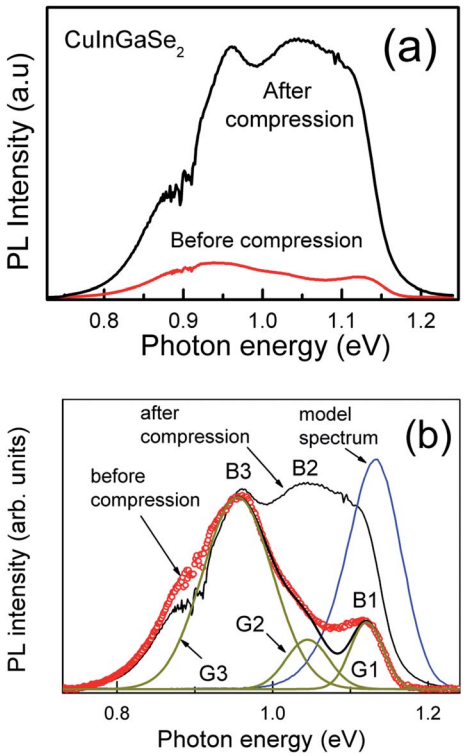

Fig. 3 (a) Comparison of the intensity of PL spectra of as-grown and compressed CIGS films (spectra recorded at 5 K). (b) The same spectra with normalized intensities in comparison with a fit of the sum of 3 gaussian shapes G1, G2, G3 for the spectrum before compression and a reference spectrum recorded at 10 K.

conversion efficiency of 15%, have been characterised using PL.[26] Their PL spectra reveal a single high intensity recombination band with its maximum at 1.13 meV and FWHM of 82 meV. The intensity of the reference spectrum is divided by a factor of 35 for comparison.

Three broad PL bands B1, B2 and B3 at about 1.12, 1.04 and 0.94 eV as well as noticeable water absorption at 0.9 eV can be seen in the spectrum before the compression. The FWHM of the B1, B2 and B3 bands are approximated as 60, 80 and 140 meV by fitting the three Gaussians G1, G2 and G3, respectively, which have been indicated in the Fig. 3b. These Gaussians fit well into the high energy slopes of the B1, B2 and B3 bands whereas the low energy ones do not quite follow that of B1, B2 and B3 demonstrating a strong asymmetry of the band shapes. The dip between G1 and G2 suggests that the spectrum may contain one or more low intensity non-resolved bands. In this report we will discuss only the three higher intensity bands B1, B2 and B3. The relative intensities of these bands vary at different points on the samples, but their spectral positions remain the same. Amongst the three bands, the spectral position of B1 is very close to the reference spectrum band. The FWHM of B1 band is also in the range of the reference film. Therefore, we can expect the defects associated with the B1 band in our samples, to be similar to that in the reference-model film. The small differences in the spectral position and FWHM can be due to the differences of the elemental composition and the structural quality, respectively.

The compression of the CIGS films generates changes in the film morphology and their electronic properties. Along with the significant increase in the total PL intensity, the compression increases the relative intensity of the higher energy part of the PL spectrum dramatically. However, the PL intensity after compression is still lower than that of the reference spectrum. The detailed investigation of the excitation power and temperature dependencies of the PL spectra will help to understand the changes in the electronic properties happened due to the compression.

Analysis of dependencies of the PL spectra on the laser excitation power can help to identify the recombination mechanisms involved. Such dependency of the PL spectra for the films before and after compression measured at 5 K for laser excitation powers ranging from 0.2 to 20 mW, are shown in Fig. 4a and b, respectively. It can be seen in Fig. 4b in the PL spectra after the compression that the B1, B2 and B3 bands are significantly less resolved, although at excitation powers below 10 mW the B3 band can be seen better resolved in both Fig. 3b and 4b. The intensity of the B1 band emission, associated with the shallower defects, grows faster at increasing excitation power resulting in almost a disappearance of the B3 band at laser excitation power of 20 mW.

The spectra measured at different excitation intensities were normalised in order to quantify changes in the B1 and B3 bands, which are better resolved in the spectra than B2. The spectra normalised to compare the B3 band spectral positions are shown in Fig. 5a. It can be seen that the B3 band shifts with

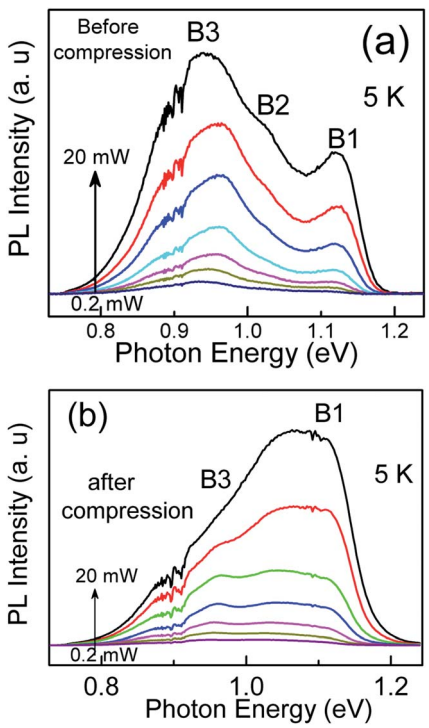

Fig. 4 (a) Dependence of the PL spectra, measured before compression with different excitation laser power. (b) Dependence of the PL spectra, measured after compression with different excitation laser power.

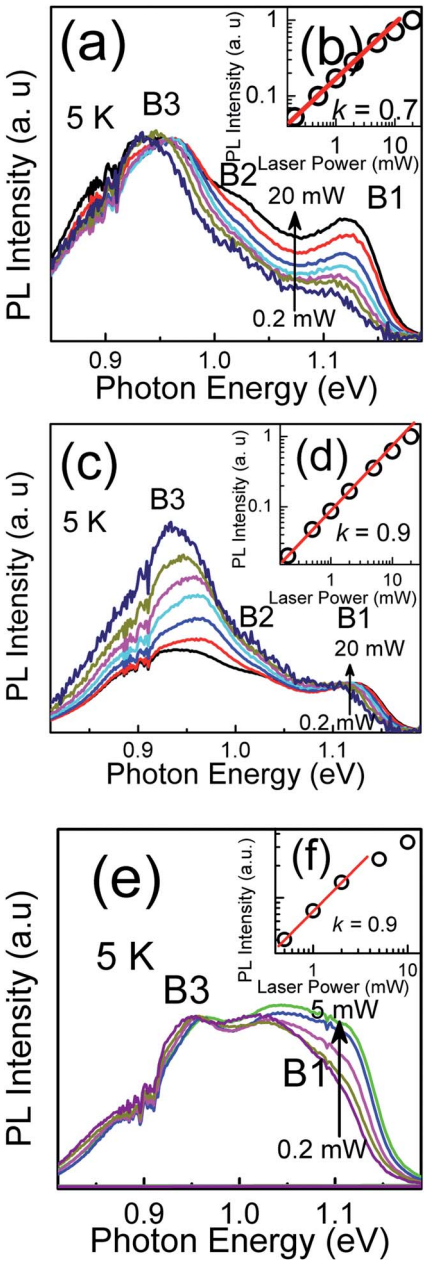

Fig. 5 Dependencies of the PL spectra on excitation laser power, measured at 5 K for the films before and after compression. (a) The spectra for the films before compression normalised to B3 band, (b) log–log dependence of the B3 band intensity on laser power. (c) The spectra for the films before compression normalised to the B1 band, (d) log–log dependence of the B1 band intensity on laser power. (e) Dependence of the PL spectra, measured after compression, on excitation laser power normalised to B3, (f) log–log dependence of the B3 band intensity on laser power.

increasing excitation power towards higher energies. The rate of the *j*-shift is 25 meV per decade of laser power change. The PL spectra equalised to analyse the B1 band shifts are shown in Fig. 5c. The B1 band also shifts with increasing excitation power towards higher energies although the rate of the *j*-shift is 14 meV per decade, which is close to that of the reference band suggesting a similarity of their nature.

Dependence of the normalised PL spectra on the laser excitation power after the compression measured at 5 K for laser excitation powers ranging from 0.2 to 20 mW is shown in Fig. 5e. The B1, B2 and B3 bands in these spectra are significantly less resolved than those before the compression. However, the *j*-shift of the B3 band can be estimated at low excitation powers. The rate of the *j*-shift for the B3 band is estimated to be about 14 meV per decade. Thus after the compression the B3 band demonstrates a significant reduction of the *j*-shift rate from 25 to 14 meV per decade.

The blue shift of PL bands with increasing excitation power is often used to identify the recombination mechanism as donor–acceptor pair (DAP) one.[27] Wave functions of closely located donors and acceptors overlap making possible the recombination of localised electrons and holes. In this case, the rate of *j*-shift cannot exceed a few meV per decade. The observed values of *j*-shift for the B1, B2 bands in this study and for the reference band exceed such a limit significantly. This suggests that the radiative recombination mechanisms of these bands are more likely to be associated with band tails generated by high concentrations of clusters of charged defects.[28,29] The asymmetrical shape of the bands showing more abrupt high energy slopes and longer low energy tails also can be taken as an evidence of band-to-tail (BT) related recombination mechanisms.[28] Such BT related transitions are often observed in PL spectra of ternary and quaternary chalcopyrite single crystals and thin films.[29–32] Spatial potential fluctuations in CIGS and related compounds are generated by clusters of charged defects. These defects are due to randomly distributed spatial deviations from the stoichiometry, and result in band tails.[28,33]

According to the theory of heavily doped semiconductors with spatial potential fluctuations[28] and its application to PL analysis[33] the radiative recombination can arise from several different channels. In p-type material, it can be the recombination of a free electron and a hole localised in the valence band tail acting like acceptor. Because of potential fluctuations each band tail can represent not a single acceptor level but a distribution of acceptor states. The mean amplitude of potential fluctuations strongly depends on the level of doping and compensation, which determines the spectral positions of the band and the *j*-shift magnitude. The greater observed *j*-shift is related to the higher potential fluctuation amplitude. It can occur through the acceptor state (band-to-impurity, BI band) that is deep enough not to overlap with the valence band tail.[34] In highly compensated semiconductor, the recombination can be between deep donor and acceptor pairs also affected by the presence of band tails.[28]

The dependencies of the PL intensity (I) on increasing laser power (P) for the B1 and B3 bands were fitted with equation $I \sim P^k$ (ref. 35) and plotted on a log–log scale in Fig. 5b and d for films before compression as well as 5f for films after compression. The slope (k) of these log–log dependencies can help to understand the nature of the transitions associated with B1 and B3. The slopes for the B3 log–log dependence before (Fig. 5b) and after (Fig. 5f) compression are measured to be $k \approx 0.7$ and $k \approx 0.9$, respectively. These k slope values are smaller than unity suggesting that the B1 and B3 bands before and after compression are associated with defect related transitions.[35] The deviations from linearity in Fig. 5b, d and f for the laser powers above 2 mW indicate that the laser beam has increased the sample temperature.

In order to study the effect of temperature, the sample temperature has been varied from 5 K to 170 K. Fig. 6 shows the effect of temperature on the PL spectra. The spectral positions of all the three bands (B1, B2 and B3) in the spectra, measured before compression shown in Fig. 6a, demonstrate shifts towards the lower energies with the temperature increase. The B1 band quenches first then the B3 band quenches whereas the B2 band quenches the least at temperatures of about 170 K. The merged bands in the PL spectra of the film measured after compression (Fig. 6b) reveal the similar trend. The central part of the spectra, where we can expect the B2 band is quenching the least whereas the higher energy part is quenching first.

The red shifts at increasing temperature are additional evidence that these transitions are associated with band tails. Such shifts have been reported for similar bands in PL spectra of thin films and single crystals.[26,29,31,32] The band in the reference spectrum also demonstrates very similar red shifts at increasing temperature, which confirms the similarity of the defect nature associated with this band.

The red shift of the bands at temperature increase, shown in Fig. 6, and significant *j*-shifts at excitation power changes

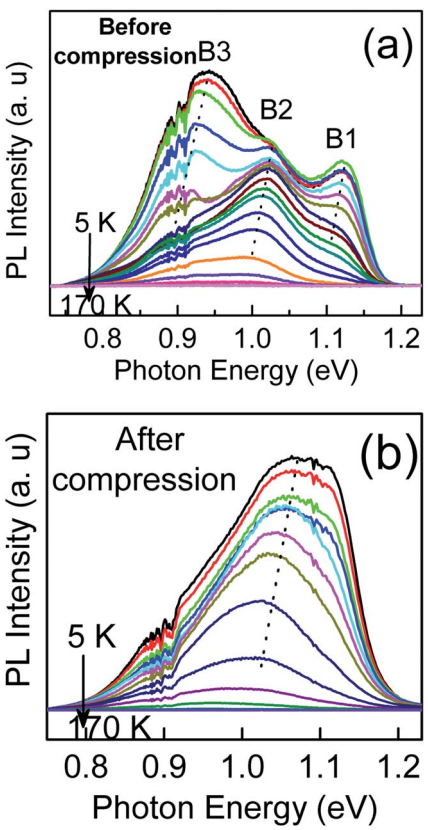

Fig. 6 (a) Dependence of the PL spectra, measured before compression on temperature. The shifts of the bands towards lower energies are shown by dot lines. (b) Dependence of the PL spectra, measured after compression, on temperature. The shifts of the bands towards lower energies are shown by dot lines.

suggest that all the three observed bands B1, B2 and B3 are associated with BT recombination. The B1 band can be preliminary assigned to BT type recombination, a recombination of free electrons in the conduction band with holes localised at valence band tail. The B2 and B3 are quite deep suggesting the presence of a range of additional deep defects and can be assigned to DAP recombination affected by the influence of band tails.

Thus the results of both the excitation intensity and temperature analysis suggest that the studied CIGS thin films are highly doped and compensated. They contain high concentrations of charged defects generating significant band tails in the films before and after the compression are associated with these band tails. The B1 band is likely to be similar to the band observed in PL spectra of the reference sample and other high quality thin films fabricated by traditional techniques[1,2] and used to fabricate high efficiency solar cells. The similarity is supported by its spectral position, FWHM, *j*-shift value and red shift at increasing temperature. However, the PL intensity of B1 is still lower than the reference sample suggesting the presence of significant non-radiative recombination and radiative recombination associated with deeper, unwanted defects. These defects are working as traps for charge carriers. Some of these defects are represented by the B2 and B3 bands. In the further improvement of the technique of compression, we will try to increase the PL intensity further.

The compression induces beneficial influences in the interfacial properties and hence in the PL spectra of the films. It increases the integrated PL intensity by an order of magnitude, suggesting a reduction of non-radiative recombination, increasing mostly the intensity of the B1 band whereas the unwanted B2 and B3 bands increase their intensity at a lower degree. The micro-structural quality improvement due to applied compression is also evident from *j*-shift from 25 meV to 14 meV per decade for the B3 band suggesting a reduction of the average depth of the potential fluctuations.

The proposed explanations of the changes in the PL spectra are based on analysis of the SEM micrographs. The branched tree structure of the grains before the compression can be seen in Fig. 1a and c. After compression, it was changed to more compact and dense columnar one. From the micrographs it looks like the compression mostly affects the position of larger grains pressing them closer to the substrate and to each other, and probably breaking some of them. This breakage reveals freshly cleaved surfaces of CIGS generating the observed high intensity the PL emission and its redistribution towards higher energy bands.

Although a comparison of the PL spectra of the CIGS films before and after compression along with the CIGS solar cell devices would have added more information to this investigation.[36] However, we are carrying out those studies systematically, which will be published elsewhere.

Conclusions

$Cu(In,Ga)Se_2$ (CIGS) thin films deposited on Mo-coated soda-lime glass substrates by selenisation of metallic precursors at 500 °C were found to be porous in nature resulting in poor efficiency values. An approach of reducing the porosity was applied by mechanically compressed at 25 MPa. The following conclusions were drawn:

(i) The compression reduces porosity without changing the preferential orientation and elemental composition.

(ii) The PL spectra reveal three broad and intense bands shifting towards higher energies (*j*-shift) at excitation power increase indicating as high level of doping and compensation. At increasing temperature the bands reveal red shifts, which is a characteristic of band tails generated by spatial potential fluctuations.

(iii) The compression increases PL intensity by an order of magnitude, mostly increasing the relative intensities of the higher energy bands suggesting a reduction of non-radiative recombination. It also reduces the *j*-shift demonstrating an improvement of the structural quality.

The above observations clearly reflect an improvement in the CIGS film quality upon compression.

Acknowledgements

This research work was partially supported by EPSRC UK-India programme (EP/H040218/1) for Advancing the Efficiency and Production Potential of Excitonic Solar Cells (APEX) and partially funded by Excitonic Supergen (EPSRC (EP(G03101088/1))) program. This research work was also partially supported by the EPSRC, Royal Society, RFBR grants 13-02-96046-ural, 11-02-00379, 10-03-96047 and 11-03-00063.

Notes and references

1 I. Repins, M. A. Contreras, B. Egaas, C. DeHart, J. Scharf, C. L. Perkins, B. To and R. Noufi, *Prog. Photovoltaics*, 2008, **16**, 235–239.
2 P. Jackson, D. Hariskos, E. Lotter, S. Paetel, R. Wuerz, R. Menner, W. Wischmann and M. Powalla, *Prog. Photovoltaics*, 2011, **19**, 894–897.
3 http://www.zsw-bw.de/.
4 C. J. Hibberd, E. Chassaing, W. Liu, D. B. Mitzi, D. Lincot and A. N. Tiwari, *Prog. Photovoltaics*, 2010, **18**, 434–452.
5 C. Guillén and J. Herrero, *Sol. Energy Mater. Sol. Cells*, 2002, **73**, 141–149.
6 S. F. Chichibu, M. Sugiyama, M. Ohbasami, A. Hayakawa, T. Mizutani, H. Nakanishi, T. Negami and T. Wada, *J. Cryst. Growth*, 2002, **243**, 404–409.
7 M. Kaelin, D. Rudmann, F. Kurdesau, H. Zogg, T. Meyer and A. N. Tiwari, *Thin Solid Films*, 2005, **480–481**, 486–490.
8 T. Wada, J. Kubo, S. Yamazoe, A. Yamada and M. Konagai, *25th European Photovoltaic Solar Energy Conference and Exhibition/5th World Conference on Photovoltaic Energy Conversion*, Valencia, Spain, 2010.
9 V. Alberts, J. Bekker, M. J. Witcomb, J. H. Schön and E. Bucher, *Thin Solid Films*, 2000, **361–362**, 432–436.
10 H. Sugimoto, Y. Kawaguchi, Y. Yasaki, T. Aramoto, Y. Tanaka, H. Hakuma, S. Kuriyagawa and K. Kushiya, *26th*

European Photovoltaic Solar Energy Conference and Exhibition, Hamburg, Germany, 2011.
11 D. L. Schulz, C. J. Curtis, A. Cram, J. L. Alleman, A. Mason, R. J. Matson, J. D. Perkins and D. S. Ginley, *Photovoltaic Specialists Conference, 1997, Conference Record of the Twenty-Sixth IEEE*, 1997.
12 A. Brummer, V. Honkimäki, P. Berwian, V. Probst, J. Palm and R. Hock, *Thin Solid Films*, 2003, **437**, 297–307.
13 M. Kaelin, D. Rudmann and A. N. Tiwari, *Solar Energy*, 2004, **77**, 749–756.
14 Z. Wei, T. Shimell and H. M. Upadhyaya, *26th European Photovoltaic Solar Energy Conference and Exhibition*, Hamburg, Germany, 2011.
15 S. Verma, N. Orbey, R. W. Birkmire and T. W. F. Russell, *Prog. Photovoltaics*, 1996, **4**, 341–353.
16 http://www.solar-frontier.com/eng/news/2013/C020760.html.
17 http://www.tsmc.com/english/solar/index.htm.
18 S. B. Zhang, S.-H. Wei, A. Zunger and H. Katayama-Yoshida, *Phys. Rev. B: Condens. Matter Mater. Phys.*, 1998, **57**, 9642–9656.
19 A. Darga, D. Mencaraglia, Z. Djebbour, A. Migan Dubois, J. F. Guillemoles, J. P. Connolly, O. Roussel, D. Lincot, B. Canava and A. Etcheberry, *Thin Solid Films*, 2009, **517**, 2550–2553.
20 D. W. Lee, M. S. Seol, D. W. Kwak, J. S. Oh, J. H. Jeong and H. Y. Cho, *Thin Solid Films*, 2012, **520**, 6382–6385.
21 M. V. Yakushev, R. W. Martin, F. Urquhart, A. V. Mudriy, H. W. Schock, J. Krustok, R. D. Pilkington, A. E. Hill and R. D. Tomlinson, *Jpn. J. Appl. Phys.*, 2000, **39S1**, 320.
22 M. V. Yakushev, R. W. Martin, J. Krustok, H. W. Schock, R. D. Pilkington, A. E. Hill and R. D. Tomlinson, *Thin Solid Films*, 2000, **361–362**, 488–493.
23 S. Senthilarasu, T. A. N. Peiris, J. García-Cañadas and K. G. U. Wijayantha, *J. Phys. Chem. C*, 2012, **116**, 19053–19061.
24 H. M. Upadhyaya, N. Hirata, S. A. Haque, M.-A. de Paoli and J. R. Durrant, *Chem. Commun.*, 2006, 877–879.
25 U. Rau and H. W. Schock, *Appl. Phys. A*, 1999, **69**, 131–147.
26 M. V. Yakushev, A. V. Mudryi, V. F. Gremenok, E. P. Zaretskaya, V. B. Zalesski, Y. Feofanov and R. W. Martin, *Thin Solid Films*, 2004, **451–452**, 133–136.
27 J. J. Hopfield, D. G. Thomas and M. Gershenzon, *Phys. Rev. Lett.*, 1963, **10**, 162–164.
28 B. I. Shklovskii and A. L. Efros, Translated by S. Luryi, *Electronic Properties of Doped Semiconductors*, Springer, Berlin, 1984.
29 P. W. Yu, *J. Appl. Phys.*, 1976, **47**, 677–684.
30 I. Dirnstorfer, M. Wagner, D. M. Hofmann, M. D. Lampert, F. Karg and B. K. Meyer, *Phys. Status Solidi A*, 1998, **168**, 163–175.
31 J. Krustok, H. Collan, M. Yakushev and K. Hjelt, *Phys. Scr.*, 1999, **1999**, 179.
32 S. A. Schumacher, J. R. Botha and V. Alberts, *J. Appl. Phys.*, 2006, **99**, 063508.
33 A. P. Levanyuk and V. V. Osipov, *Phys.–Usp.*, 1981, **24**, 187.
34 A. Jagomägi, J. Krustok, J. Raudoja, M. Grossberg, M. Danilson and M. Yakushev, *Phys. B*, 2003, **337**, 369–374.
35 T. Schmidt, K. Lischka and W. Zulehner, *Phys. Rev. B: Condens. Matter Mater. Phys.*, 1992, **45**, 8989–8994.
36 S. Shirakata and T. Nakada, *Thin Solid Films*, 2007, **515**, 6151–6154.